Optimization of Er^{3+} doped glass used as optical fiber amplifier (EDFA) for telecommunication applications

Badr Y. A., Mahmoud F. M., and Ibrahim. S. M.

Laser Science and Interaction Department, National Institute of Laser Enhanced Science, Cairo University, Cairo, Egypt.
ibrahim_maged83@yahoo.com

Abstract: The Er^{3+}:Yb^{3+} co-doped potassium-lead-germanate glass with optimum ratio 0.5 mol. % of Er^{3+} and 2.5 mol. % of Yb^{3+} (1:5) was prepared by using the conventional melting and quenching method. Raman spectroscopy and FT-IR were used to study the structure and the vibrational modes of this glass. Measurement of Raman spectroscopy showed that the maximum phonon energy of this glass was approximately 811 cm^{-1}. Optical absorption was measured to make it easy to choose the pump wavelength. X-ray diffraction confirmed that there were no periodic arrangements in the glass; i.e. it was amorphous. Differential thermal confirmed the thermal stability of this glass. The two probe method was used to investigate the electrical behavior and to measure the DC-conductivity and its temperature dependence. The introduced here system was designed using a longitudinal pumping source of 808 nm diode laser at different powers and the diagnoses of the system output was measured by double monochromator (SpectraPro 500i of ACTON) in the range of 790-1800 nm. The system output was found to increase with increasing the pumping power. The emission of the rod showed strong line at about 1600 nm. This might confirm that the proposed here design of Er-glass laser can be used in telecommunication applications.
[Badr Y. A., Mahmoud F. M., and Ibrahim. S. M. **Optimization of Er^{3+} doped glass used as optical fiber amplifier (EDFA) for telecommunication applications.** *J Am Sci* 2013; 9(10):1-12] (ISSN: 1545-1003). http://www.jofamericanscience.org. 1

Keywords: Er^{3+}:Yb^{3+}co-doped potassium-lead-germanate glass , Er-glass laser

1. Introduction:

The recent interest in optical amplifiers and lasers based on rare earth doped fibers has stimulated a new look at fiber fabrication methods. The use of optical fiber to reduce the required pump power for gain in glass lasers and amplifiers was first demonstrated in the early 1960s by Snitzer and co-workers; revisited in the 1970s by Stone and Burrus, it has been pursued with vigor since 1985. The rebirth of this field has been stimulated primarily by the application of optical amplifiers and fiber lasers to optical communications. [1]

Fabrication of suitable erbium-doped fiber is one of the keys to creating an appropriate amplifier for a particular application. Fortunately, many of the methods used in fabricating low-loss silica transmission fiber. In most cases the concentration of erbium is low enough that the fabrication methods do not entail a significant change in the fundamental structure of the underlying glass host. [2]

Rare earth doped fibers can be fabricated by a wide variety of methods, each suited for different amplifier design needs. The concentration of rare earth dopant ranges from very high (thousands of ppm) in multicomponent glasses, to less than 1 ppm in distributed erbium doped fibers. The background losses are comparable to state-of-the-art transmission grade fiber. The methods used to fabricate rare earth doped optical fiber are, in general, variations on the techniques used to produce low-loss communications grade fiber. [2]

New compositions that offer improved amplifier performance be it from a geometry or a host composition perspective, will continue to challenge the techniques of fabrication. Commercialization of erbium-doped fiber amplifiers has required greater attention to reproducibility of core and fiber geometry, as well as dopant control to assure uniformity of doping along the longitudinal and transverse fiber axes. [2]

2. Materials and methods:

We use this potassium-lead-germanate glass because it has high; mechanical strength, chemical durability, thermal stability, refractive index, and transmission in the IR range.

2.1 Preparation method:

The glass hosts with composition (in mol. %): $70GeO_2$-20PbO-$10K_2O$ where doped with a fixed concentrations of Er^{3+} (0.5 mol. %) and Yb^{3+} (2.5 mol. %).

Melting the combination of the individual raw materials at high temperature to form a molten glass is the central phase in the production of glass. There are numerous ways to melt glass in our work we use the conventional melting. The well mixed powders were melted in a covered platinum crucible in an electric furnace (Carbolite furnace, RHF 14/9) at 1320 °C temperature for 20 min.

2.2 Rod preparation:

Some of the melts were poured and rapidly quenched by pressing between two stainless steel plates kept at the room temperature for diagnoses processes. The remaining quantity of the melts was poured in a cylinder with a hole of 5 mm diameter and 2.5 cm length to make the rod as shown in Fig.(1). Some pieces of the glass were polished carefully for resistivity and refractive index measurements. Some pieces were grounded well in an agate mortar for the x-ray diffraction and differential thermal analysis (DTA) measurements. The rod was polished carefully from its ends to be used in the amplifier.

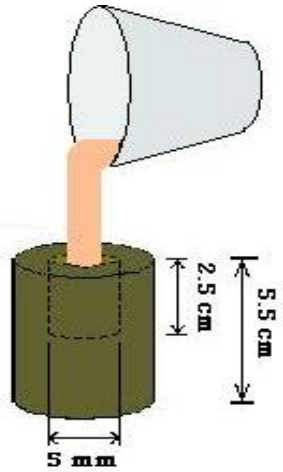

Fig.(1): Pouring process of the rod.

2.3 Methods of investigation

2.3.1 Measurements of Fourier Transform infrared (FT-IR) spectra:

FTIR is most useful for identifying chemicals that are either organic or inorganic. It can be utilized to quantitate some components of an unknown mixture. The FT-IR spectrometer (Bruker, IFS 66/S) used in the spectral range of 400-4000 cm^{-1} at room temperature and the measurements were obtained under the condition of dried air to avoid the IR absorption by water or CO_2 vapors. The IR spectra of the samples were taken on pressed KBr pellets. 2 mg of each sample were ground with 100 mg of KBr into a fine powder and pressed into pellets.

2.3.2 Measurement of Fourier Transform Raman spectrum:

Raman scattering spectrum of the doped glass sample was recorded with a FT-Raman spectrometer (Nicolet 670), in the 100 - 1500 cm^{-1} spectral range at room temperature.

The excitation source is Nd^{3+}:YAG laser of wavelength 1064 nm with a maximum power of 2W. The laser beam is passed through the sample. Then light scattered sideways from the sample is collected by a lens and passed into an FT-interferometer to be analyzed into its components. The signal is detected by a sensitive InGaAs detector and after amplification, it is processed by a computer which plots the Raman spectrum.

2.3.3 Measurements of optical absorption:

Near UV/visible/near IR absorption spectra of glass samples were obtained with Shimadzu (UV-3101PC) double-beam spectrophotometer in the spectral range of 350-1700 nm.

2.3.4 Fluorescence (normal emission)

The excitation source was Argon ion Ar^+ laser (LEXEL 95) of wavelength 488 nm with a power of 150 mW. The emitted light from the sample is collected by a lens and focused on the entrance slit of a grating monochromator (Spex 750m) to be resolved into its component wavelengths.

The light emerging from the monochromator is detected with a photomultiplier detector with associated high-voltage power supplies. The photomultiplier tube converts the optical signal into an electrical signal, which is then recorded and amplified by a lock-in amplifier (SR 510). The scan drive component is controlled by computer software and allows the monochromator to turn so that all wavelengths of the emitted light are swept (or scanned) across the exit slit to the detector.

2.3.5 X-ray diffraction

The amorphous nature of the glass sample was examined by x-ray powder diffraction using CuK_α radiation at λ= 1.54Å (Scintag, advanced diffraction system) with nickel filter, over 2θ range of 3-70º.

2.3.6 Differential Thermal Analysis (DTA)

DTA instrument measures the difference in temperature between the sample and the reference

material, which are exposed to the same heating schedule via symmetric placement with respect to the furnace. From the DTA curve the crystallization and glass transitions temperature were measured and the thermal stability factor ΔT was calculated. The DTA measurements were performed with a differential thermal analyzer (Shimadzu DTA-50 detector) at a heating rate of 10 °C/min under nitrogen atmosphere with 30 ml/min flow rate in the temperature range of 10-800 °C. About 50 mg of the powdered glass was loaded in sample crucible and similar quantity of fired Al_2O_3 was used in the reference way of the analyzer.

2.3.7 D.C. conductivity

We used the two probe method to observe the temperature dependence of DC conductivity for our sample. We make a silver conducting paint on the polished faces of the glass sheet used then situated them between two copper electrodes. The used dc voltage is 24V. We measure the temperature with heating rate of 5K/min from 312-625 K range using thermocouples.

To calculate the DC conductivity σ of the sample we use the relation:

$$\sigma = Id/VA \text{ ---------- (1)}$$

Where d is the thickness of the sample, A is the area of the paint on the sample, V is the voltage applied between the two faces of the sample, and I is the measured current.

2.4 Setup specifications

The setup consists of two mirrors, rod, and IR laser. Fig.(2) shows the complete diagram of setup used.

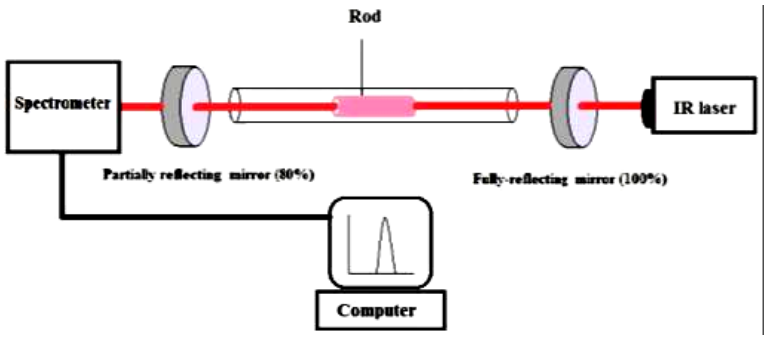

Fig.(2): The setup used.

For the detection process we used SpectraPro 500i of ACTON spectrometer. And we use a laser diode of 808 nm wavelength and power of 50 w for the pumping process. The characteristic curve of this laser is shown in Fig(3).

There are two plane mirrors of 0.5 inch diameter and 0.25 inch thickness used for the cavity resonator. The rear mirror must be fully-reflecting (100%) and the front mirror partially reflecting (80%). The characteristics of these mirrors are shown in Figs.(4.a and b).

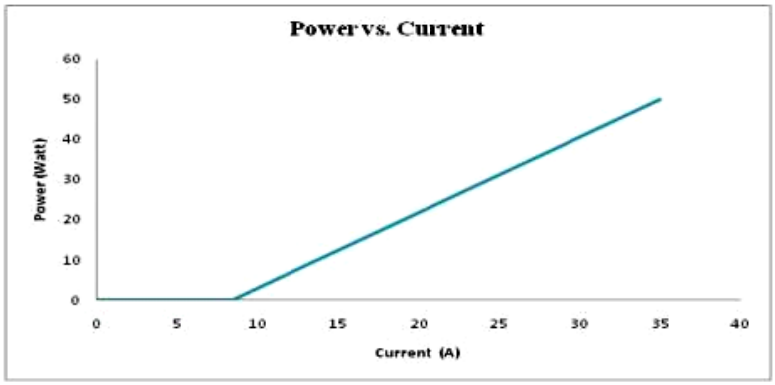

Fig.(3): The setup used Longitudinal pumping.

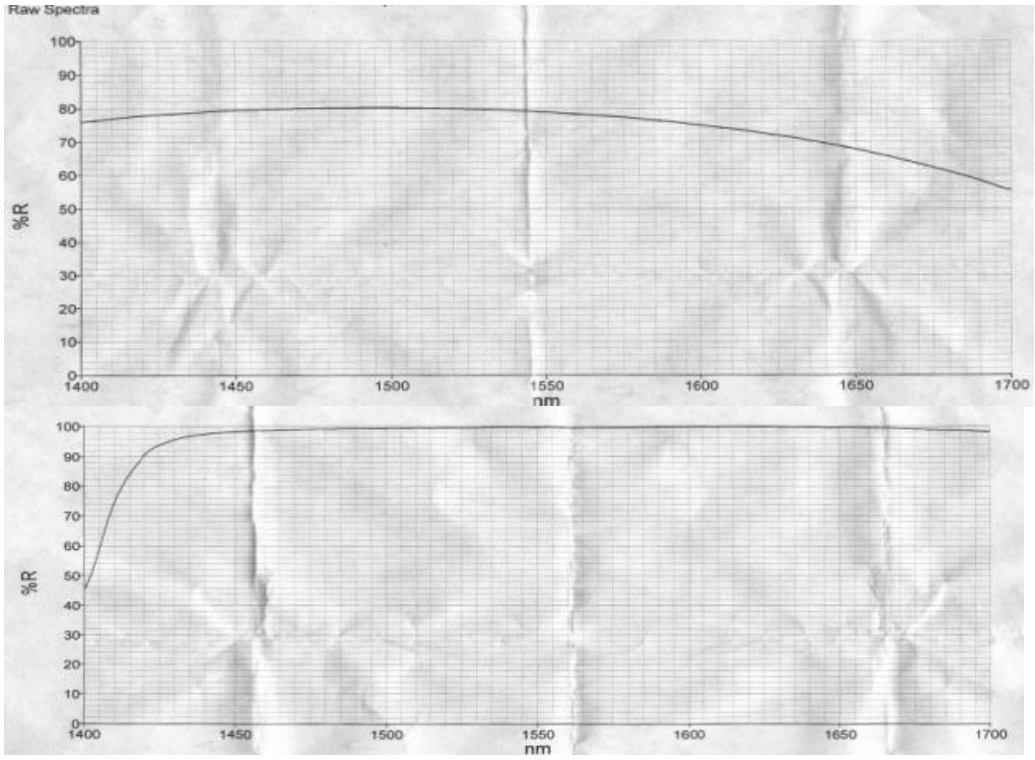

Fig.(4.a): Characteristics of the reflecting face of 80%R mirror at 1540 nm.
Fig.(4.b): Characteristics of the reflecting face of 100%R mirror at 1540 nm.

3. Results and Discussion:

It is well known that the role of host material in the performance of solid state lasers is fundamental mainly for mechanical, thermal and specially optical properties of the host. In order to optimize the introduced here Er^{3+}-doped glass laser and amplifier we thought that it is worth. While to start with first, the glass matrix hosting both Er^{3+} and Yb^{3+} aiming to achieve the optimum structure of this matrix yielding the best optical, mechanical, and thermal properties of this matrix. In one of our previous work [3] (*Study of some oxide-based glasses doped with rare earth ions*) we justified that the best structure was $70GeO_2$-$20PbO$-$10K_2O$. Second, what is the concentration of the Er^{3+} and Yb^{3+} in the host material? It was found that the best concentration from five different concentrations (Er^{3+}: Yb^{3+}; 1:0, 1:1, 1:3: 1:5) was 1:5 concentration of Er^{3+}: Yb^{3+} respectively. [3]

3.1 Characterization of the obtained glass and rod

3.1.1 Measurements of Fourier Transform infrared (FT-IR) spectra

The FT-IR absorption spectrum of the doped $G_{70}P_{20}K_{10}$ glass sample dispersed in KBr pellet, in the spectral range of 400-1400 cm^{-1} at room temperature, is shown in Fig.(5). The spectrum is dominated by a band centered at around 788 cm^{-1}, with other bands centered at around 410, 550, and shoulder at 974cm^{-1}. These bands are interpreted as follows: The band at around 410 cm^{-1} could be attributed to the Ge-O-Pb bridging vibrations, while the band at around 550 cm^{-1} is assigned to the symmetric stretching of oxygen atoms in the Ge-O-Ge bridges [4]. The high-frequency band at 788 cm^{-1} could be assigned to the symmetric stretching mode of Ge-O- bond with non-bridge oxygen [5].

The shoulder at around 974 cm^{-1} could be assigned to the asymmetric stretching vibration mode of Ge-O-Ge bridges connecting [GeO_4] tetrahedral. [6, 7]

3.1.2 Measurement of Fourier Transform Raman spectrum:

The Raman spectrum of the undoped $G_{70}P_{20}K_{10}$ glass obtained at room temperature in the spectral range of 100-1200 cm^{-1} is shown in Fig.(6).

The Raman spectrum is deconvoluted using Gaussian distribution to four bands centered at around 209, 333, 529, and 811 cm^{-1}. By considering the features of Raman scattering spectra for many reported GeO_2-based glasses, the spectrum for the undoped $G_{70}P_{20}K_{10}$ glass is interpreted as follows: The low-frequency band at around 209 cm^{-1} could be attributed to vibrations involving the heavy metal atoms Pb. [8] The band at around 333 cm^{-1} is assigned to the vibrations of Ge-O-Pb bridges. [8-10]

The intermediate-frequency band at around 529 cm^{-1} is assigned to the symmetric stretching vibrations of Ge-O-Ge bridges connecting [GeO_4] tetrahedra. [8, 6, 11] The high-frequency band at around 811 cm^{-1} is assigned to the symmetric stretching mode of the [GeO_4] tetrahedron with one non-bridge oxygen (i.e., $Ge-O^-$ bond). [6, 11]

Difference between IR and Raman spectra

There are some differences between IR and Raman spectra such as the width of the bands; they are sharper in Raman than in IR. The second difference is the shift between Raman and IR bands. The third difference is that the Raman spectrum measurement depends on scattering but IR depends on absorption.

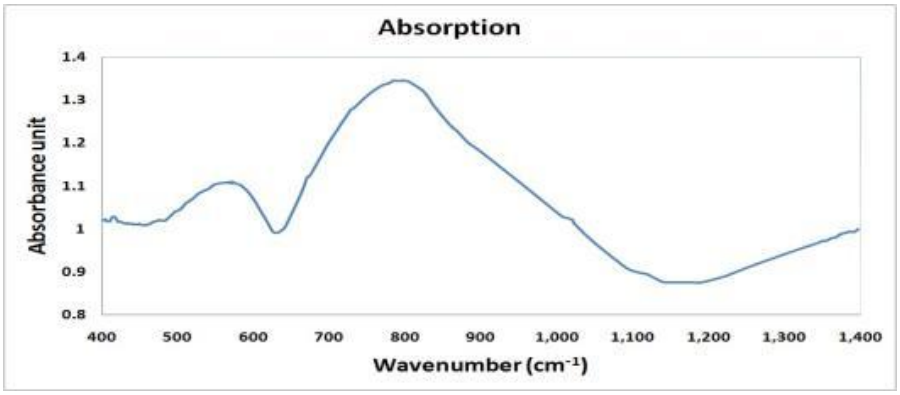

Fig.(5): The FT-IR absorption spectra of the Er^{3+}/Yb^{3+} co-doped glasses with 1:5 Er^{3+}:Yb^{3+} concentration ratio.

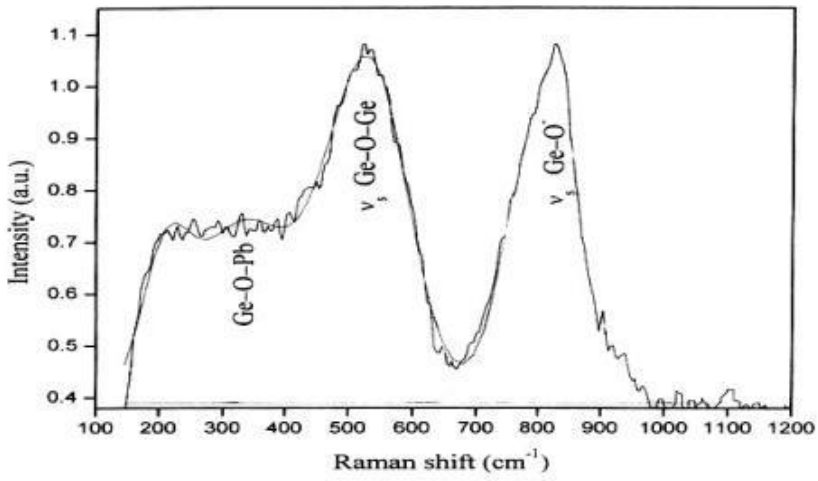

Fig.(6): The Raman spectrum of the undoped $G_{70}P_{20}K_{10}$ glass as measured in our lab. [3]

3.1.3 Measurements of optical absorption:

The absorption spectra of the Er^{3+}/Yb^{3+} co-doped $G_{70}P_{20}K_{10}$ glasses with 1:5 Er^{3+}:Yb^{3+}concentration ratio, in the 350-1700 nm spectral range at room temperature, are shown in Fig.(7). The absorption spectra consist of a number of inhomogeneously broadened bands attributed to transitions occurring within the 4f- shell of the rare earth ions. [12] The broadening of the absorption bands is attributed to the amorphous nature (absence of long-range order) of the glass host. That is, in a glassy matrix, the local environment around the rare earth ions varies from site to site, leading to variations in the ligand field. This results in slight broadening of the energy levels. [13-15] Table (1) lists the absorption peaks and the corresponding assigned transitions. [16- 18]

The unique absorption band of Yb^{3+} ions (at around 976 nm) corresponds to the $^2F_{7/2} \rightarrow {}^2F_{5/2}$

transition and overlaps that of Er^{3+} ions for the $^4I_{15/2} \rightarrow {}^4I_{11/2}$ transition. Compared to Er^{3+} ions, the absorption of Yb^{3+} near 976 nm is predominant due to the high absorption cross-section of Yb^{3+} ions at this wavelength. [12, 19-24]

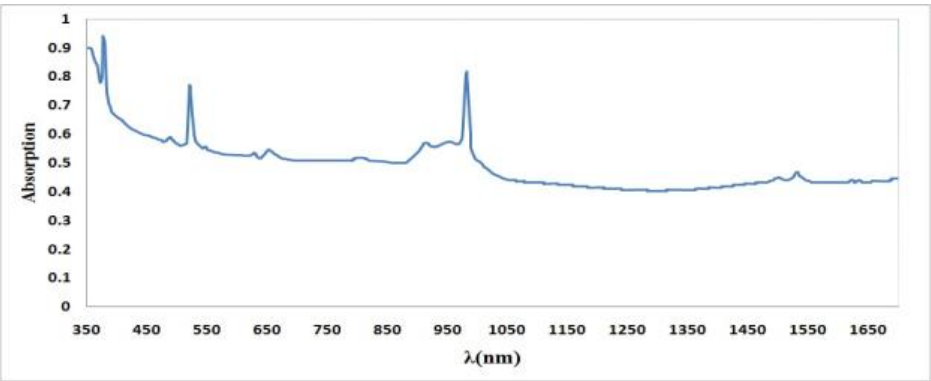

Fig. (7): The absorption spectra of Er^{3+}/Yb^{3+} co-doped $G_{70}P_{20}K_{10}$ glasses with 1:5 Er^{3+}:Yb^{3+}concentration ratio.

Since there is only one electronic excited state for Yb^{3+} ions (the $^2F_{5/2}$ state), when a diode laser at around 976 nm is used to excite the Yb^{3+} ions, the emission from the $^2F_{5/2}$ state of Yb^{3+} overlaps the absorption band for the $^4I_{15/2} \rightarrow {}^4I_{11/2}$ transition of Er^{3+} ions. This results in an efficient resonant-energy transfer (ET) from Yb^{3+} to Er^{3+} ions in the Yb^{3+}/ Er^{3+} co-doped systems. Hence, the addition of Yb^{3+} to Er^{3+}-doped glass can enhance the pumping efficiency of 977 nm diode laser indirectly through the energy transfer (ET) fromYb^{3+} to Er^{3+}. [20, 21, 24]

Table (1): The absorption peaks and the corresponding assigned transitions.

Peak position λ(nm)	Average Energy (cm^{-1})	Assigned transition
378	26455	$(Er^{3+})\ ^4I_{15/2} \rightarrow {}^4G_{11/2}$
488	20492	$(Er^{3+})\ ^4I_{15/2} \rightarrow {}^4F_{7/2}$
522	19157	$(Er^{3+})\ ^4I_{15/2} \rightarrow {}^2H_{11/2}$
546	18315	$(Er^{3+})\ ^4I_{15/2} \rightarrow {}^4S_{3/2}$
652	15337	$(Er^{3+})\ ^4I_{15/2} \rightarrow {}^4F_{9/2}$
800	12500	$(Er^{3+})\ ^4I_{15/2} \rightarrow {}^4I_{9/2}$
976	10246	$(Er^{3+})\ ^4I_{15/2} \rightarrow {}^4I_{11/2}$ and $(Yb^{3+})\ ^2F_{7/2} \rightarrow {}^2F_{5/2}$
1535	6514	$(Er^{3+})\ ^4I_{15/2} \rightarrow {}^4I_{13/2}$

3.1.4 Fluorescence (normal emission)

The normal emission spectrum of the Er^{3+}/Yb^{3+} co-doped $G_{70}P_{20}K_{10}$ glass (sample 1:5), obtained under excitation at 488 nm of Ar^+ laser with a power of 150 mW of the range 520-700 nm is shown in Fig.(8).

Intense green and very week red emission bands centered at around 532, 546, and 655 nm are observed and assigned to the $^2H_{11/2} \rightarrow {}^4I_{15/2}$, $^4S_{3/2} \rightarrow {}^4I_{15/2}$ and $^4F_{9/2} \rightarrow {}^4I_{15/2}$ transitions of Er^{3+} ions, respectively. [25, 13, 16] Based on the simplified energy levels of Er^{3+} ions in $G_{70}P_{20}K_{10}$ glass presented in Fig.(9) and the energy matching, the 532, 546, and 655 nm emission bands are interpreted as follows:

Initially, the ground state absorption (GSA) of pump photons (488 nm) excites the Er^{3+} ions to the $^4F_{7/2}$ level, from which, fast multiphonon relaxation (MPR) to the $^2H_{11/2}$ and $^4S_{3/2}$ levels occurs because of the small energy gap between them (~1330 cm^{-1}). The energy gap between the $^2H_{11/2}$ and $^4S_{3/2}$ levels is very small (~840 cm^{-1}), and a rapid thermal equilibrium is established between the thermally coupled $^2H_{11/2}$ and $^4S_{3/2}$ levels. The $^4F_{9/2}$ level populates from $^4S_{3/2}$ through multiphonon relaxation.

However, the energy gap between $^4S_{3/2}$ and $^4F_{9/2}$ levels is about 3047 cm^{-1}, and Raman spectrum shows that the maximum phonon energy of the glass network is ~ 811 cm^{-1}. Therefore, 4 phonons are required to bridge the gap. Hence, the multiphonon relaxation from the $^4S_{3/2}$ state occurs with a small rate. As a result, the population in $^4F_{9/2}$ level is very small. This explains why the red emission band is very week. Then, the radiative decays (RD) from these excited $^2H_{11/2}$, $^4S_{3/2}$ and $^4F_{9/2}$ levels to the ground state $^4I_{15/2}$ produce the 532, 546 and 655 nm emission bands, respectively. The above processes could be visualized as in table (2).

Table (2): Summary of all transitions

$^4I_{15/2}$ (Er^{3+}) + a pump photon (488 nm) → $^4F_{7/2}$ (Er^{3+})	(GSA)
$^4F_{7/2}$ (Er^{3+}) → $^2H_{11/2}$ (Er^{3+}), $^4S_{3/2}$ (Er^{3+})	(MPR)
$^4S_{3/2}$ (Er^{3+}) → $^4F_{9/2}$ (Er^{3+})	(MPR)
$^2H_{11/2}$ (Er^{3+}) → $^4I_{15/2}$ (Er^{3+}) + emitted photon (532nm)	(RD)
$^4S_{3/2}$ (Er^{3+}) → $^4I_{15/2}$ (Er^{3+}) + emitted photon (546nm)	(RD)
$^4F_{9/2}$ (Er^{3+}) → $^4I_{15/2}$ (Er^{3+}) + emitted photon (655nm)	(RD)

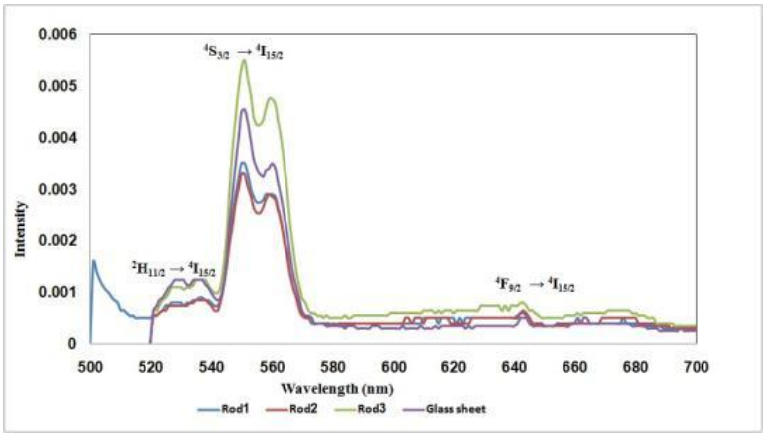

Fig. (8): The emission spectrum of Er^{3+}/Yb^{3+}co-doped $G_{70}P_{20}K_{10}$ glass under excitation at 488 nm of Ar^+ laser with a power of l50 mW.

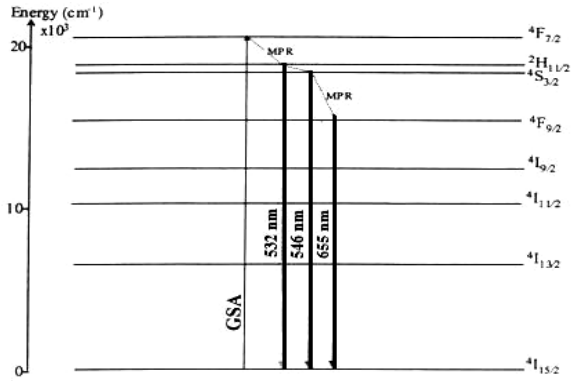

Fig.(9): The Simplified energy level diagram of Er^{3+} ions in $G_{70}P_{20}K_{10}$ glass. [23]

3.1.5 X-ray Diffraction

Fig.(10) shows the x-ray diffraction (XRD) patterns of the Er^{3+}/Yb^{3+} co-doped $G_{70}P_{20}K_{10}$ glasses with 1:5 Er^{3+}:Yb^{3+} concentration ratio. The diffuseness of the XRD patterns and the absence of detectable sharp crystalline peaks confirm the amorphous nature of all glass samples.

3.1.6 Differential Thermal Analysis (DTA)

The DTA measurements were performed with a differential thermal analyzer (Shimadzu DTA-50 detector) at a heating rate of 10 °C/min under nitrogen atmosphere in the temperature range of 10-800 °C. The DTA curve of the Er^{3+}/Yb^{3+} co-doped $G_{70}P_{20}K_{10}$ glass is shown in Figs.(11.a, b). From the figure the glass transition (onset T_g =541°C), the crystallization transition (onset T_x = 692°C), and the thermal stability factor $\Delta T = T_x - T_g$ = 151°C.

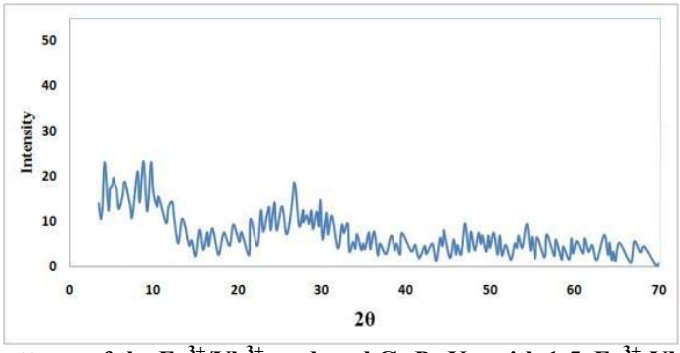

Fig.(10): The XRD patterns of the Er^{3+}/Yb^{3+} co-doped $G_{70}P_{20}K_{10}$ with 1:5 Er^{3+}:Yb^{3+} concentration ratio.

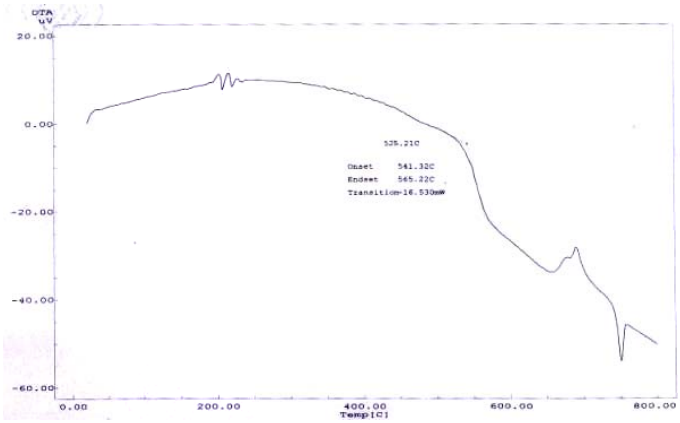

Fig.(11.a): The DTA curve of the Er^{3+}/Yb^{3+} co-doped $G_{70}P_{20}K_{10}$ glass sample from 0-800ºC.

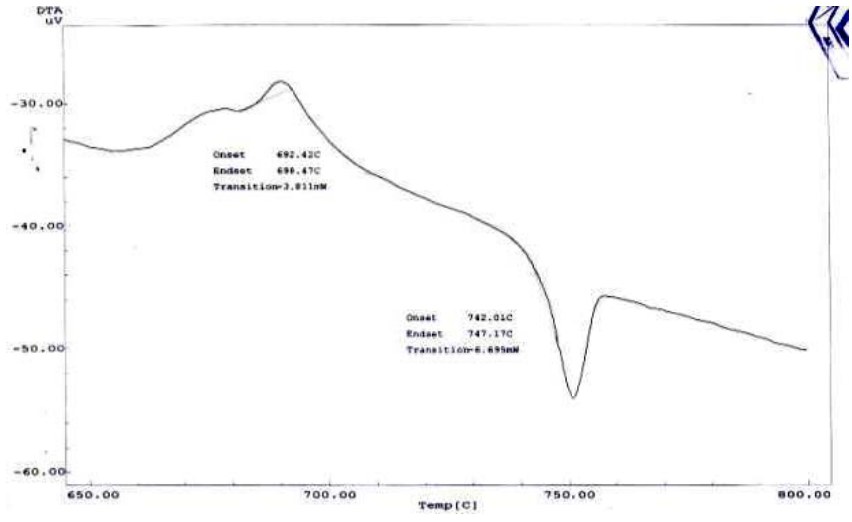

Fig. (11.b) The DTA curve of the Er^{3+}/Yb^{3+} co-doped $G_{70}P_{20}K_{10}$ glass sample from 650-800ºC.

3.1.7 D.C. Conductivity

The D.C. conductivity σ in these $G_{70}P_{20}K_{10}$ glasses may be basically attributed to the thermally activated ionic conduction of the mobile K^+ ions by surmounting the potential barrier E_a, [26] in addition to the electron hopping mechanism known for semiconducting oxide glasses. The activation energy E_a is obtained from the slope of the ln σ versus 1/T plot (the Arrhenius plot): [27]

$$\sigma = \sigma_o \exp\left(-\frac{E_a}{k_B T}\right) \quad \text{---------- (2)}$$

where σ_o is the pre-exponential factor, k_B is the Boltzmann constant, T the absolute temperature, and E_a the activation energy for conduction (the average potential energy barriers that the charge carrier must overcome in its jumps).

The temperature dependence of the DC conductivity σ in the temperature range of 312 - 625 K for Er^{3+}/Yb^{3+} co-doped $G_{70}P_{20}K_{10}$ glasses with Er^{3+}:Yb^{3+} concentration ratio of 1:5 is shown in Fig.(12) as plot of ln σ versus reciprocal of absolute temperature T. The activation energy at two different temperatures is as follow; at 320K ($\sigma = 1.27\times10^{-12}$ $\Omega^{-1}m^{-1}$) and at 420K ($\sigma = 8.25\times10^{-10}$ $\Omega^{-1}m^{-1}$) E_a=1.35 eV.

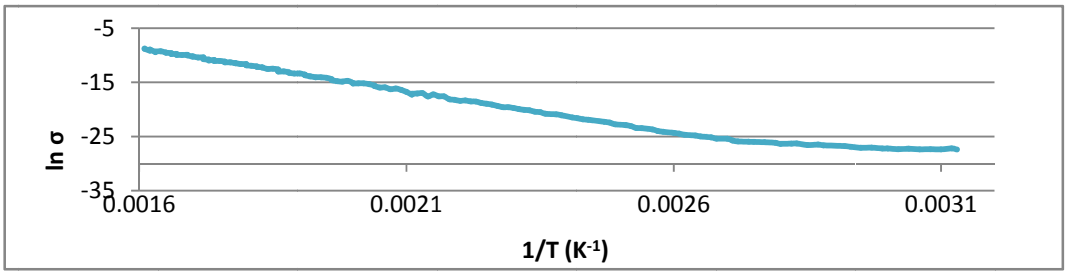

Fig. (12): Plot of ln σ versus reciprocal of absolute temperature T.

3.2 Diagnoses of Er^{3+}/Yb^{3+} glass laser

The transparency of the glass in fiber can be divided into five (six) windows (all with reduced attenuation of light) at around 850, 1310, 1390, 1550 and 1610 nm, respectively (and in the future maybe up to 1700 nm). [28]

Diode laser type LIMO class IV with LDD50 driver of wavelength 780-1000 nm and 808 nm at room temperature with power of 50 watt Quasi-cw was used here for longitudinal pumping. The obtained here is Er/Yb co-doped glass laser. The first three lines at 808, 880, 1088 nm were the outputs from the pump laser. The emission of the rod showed strong line at 1610 nm. This might confirm that the proposed here design of Er-glass laser can be used in Telecommunication applications. Fig.(13.a, b, c, and d) show the system output in semi-log scale at different pumping power and table (3) shows the output power from the system vs. the pumping power.

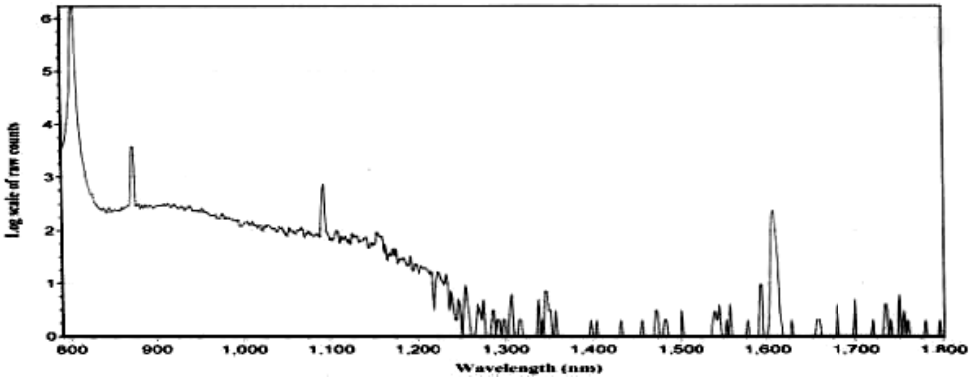

Fig.(13. a): System output at pumping power of 12.5 Watt.

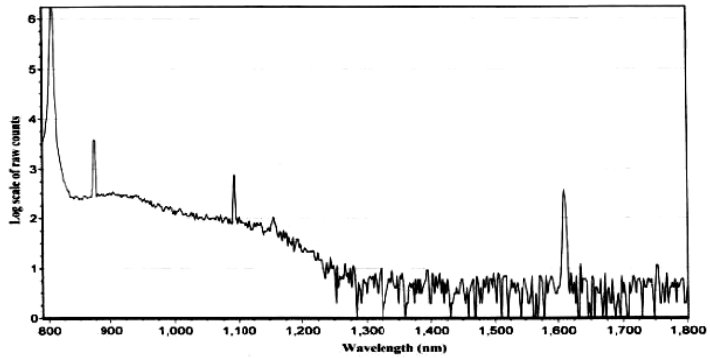

Fig.(13.b): System output at pumping power of 21.75 Watt.

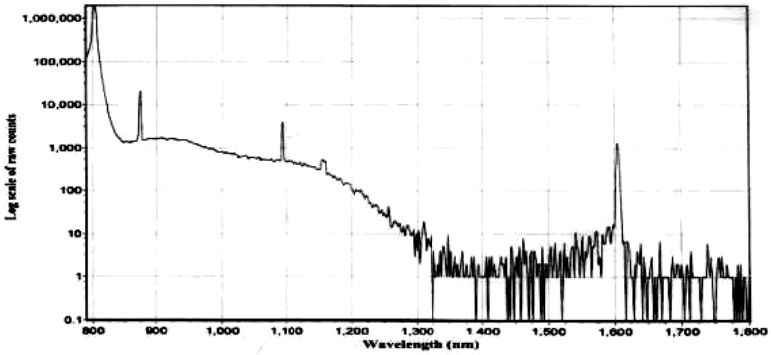

Fig.(13.c): System output at pumping power of 40.5 Watt.

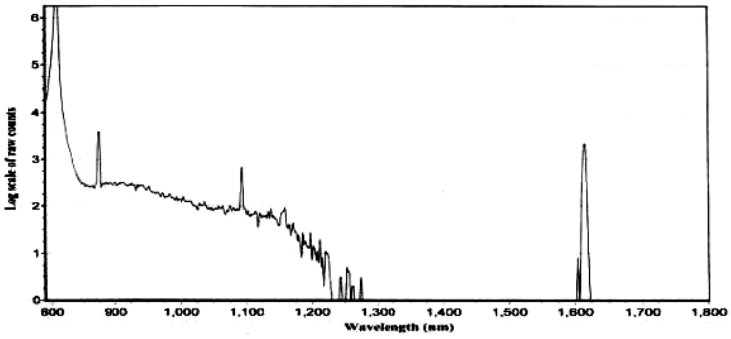

Fig.(13.d): System output at pumping power of 50 Watt.

Table (3) The output power from the system vs. the pumping power.

Fig. number	Pumping power (W)	Output power (mW)
13.a	12.5 (Threshold)	2.37
13.b	21.75	3.36
13.c	40.5	21.22
13.d	50	202.6

3.3 System applications

We used a home-made setup to test this possibility either for the rod itself or fiber obtained during the fabrication of the glass. Our results showed that both forms of Er doped glass can be used safely in the amplification process in communication. Fig.(14) shows the setup used.

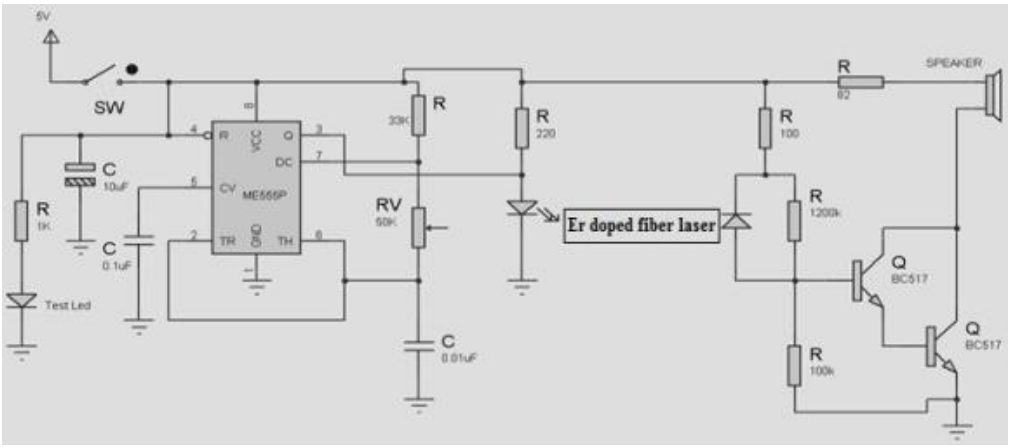

Fig.(14): The setup used.

Conclusion

1. The conventional melting and quenching method were used in the preparation of the Er^{3+}:Yb^{3+} co-doped potassium-lead-germanate ($70GeO_2$-$20PbO$-$10K_2O$) glass with optimum ratio 0.5 mol. % of Er^{3+} and 2.5 mol. % of Yb^{3+} (1:5).
2. Raman spectroscopy and FT-IR were used to study the structure and the vibrational modes of this glass. Measurement of Raman spectroscopy showed that the maximum phonon energy of the un-doped glass was approximately 811 cm^{-1}. The FT-IR measurements showed that the spectrum was dominated by a band centered at around 788 cm^{-1}, with other bands centered at around 410, 550, and shoulder at 974 cm^{-1}.
3. Optical absorption showed that the addition of Yb^{3+} to Er^{3+}-doped glass can enhance the pumping efficiency through the energy transfer (ET) fromYb^{3+} to Er^{3+}.
4. X-ray diffraction confirmed that there were no crystallization peaks or no periodic arrangements in the glass; i.e. it was amorphous.
5. Differential thermal confirmed the thermal stability of this glass. It showed that the thermal stability factor $\Delta T = T_x - T_g = 151°C$.
6. The two probe method was used to investigate the electrical behavior and to measure the DC-conductivity and its temperature dependence. It showed that the activation energy at two different temperatures is as follow; at 320K ($\sigma = 1.27x10^{-12}\ \Omega^{-1}m^{-1}$) and at 420K ($\sigma = 8.25x10^{-10}\ \Omega^{-1}m^{-1}$) E_a=1.35 eV.
7. The introduced here system was designed using a longitudinal pumping source of 808 nm diode laser at different powers and the diagnoses of the system output was done in the range of 790-1800 nm. The system output was found to increase with increasing the pumping power.
8. The emission of the rod showed strong line at 1610 nm. This might confirm that the proposed here design of Er-glass laser can be used in telecommunication applications.
9. A home-made setup was used to test the possibility for the fiber obtained during the fabrication of the glass to be used in communication.

The results showed that the Er doped glass can be used safely in the amplification process in communication.

References

1. Michel J. F. Digonnet, *"Rare Earth Doped Fiber Lasers and Amplifiers"*, 2nd Edition, Marcel Dekker, Inc., (2002).
2. Becker P. C., N. A. Olsson, J. R. Simpson, *"Erbium Doped Fiber Amplifiers"*, 2nd Edition, Academic press, San Diego London Boston, (1999).
3. Samah Mohamed H., *"Study of some oxide-based glasses doped with rare earth ions"*, Master from Cairo University (2007).
4. Qiuhua Nie, Cheng Jiang, Xunsi Wang, Tiefeng Xu, Haoquan Li, *"Frequency upconversion properties of Er^{3+}/Yb^{3+}-codoped lead-germanium-bismuth oxide glasses"*, Materials Research Bulletin 41(2006) 1496-1502.
5. Youngsik Kim, Jason Saienga, Steve W. Martin, *"Glass formation in and structural investigation of $Li_2S + GeS_2 + GeO_2$ composition using Raman and IR spectroscopy"*. Journal of Non-Crystalline Solids 351 (2005) 3716-3724.
6. Fukushima T., Y. Benino, T. Fujiwara, V. Dimitrov, T. Komatsu, *"Electronic polarizability and crystallization of K_2O-TiO_2-GeO_2 glasses with high TiO_2 contents"*. Journal of Solid State Chemistry 179 (2006) 3949-3957.
7. Jenn-Shing Wang, Kuen-Ming Hon, Ko-Ho Yang, Moo-Chin Wang, Min-Hsiung Hon, *"Mixed alkali effect on calcium aluminogermanate glasses"*. Ceramics International 23 (1997) 153-157.

8. Hongtao Sun, Junjie Yang, Liyan Zhang, Junjie Zhang, Lili Hu, Zhonghong Jiang, *"Composition dependent frequency upconversion luminescence in Er^{3+}-doped oxychloride germanate glasses"*. Solid State Communications 133 (2005) 753-757.
9. Hongtao Sun, Lili Hu, Chunlei Yu, Gang Zhou, Zhongchao Duan, Junjie Zhang, Zhonghong Jiang, *"Investigation of the effect of fluoride ions introduction on structural, OH^- content and up-conversion luminescence properties in Er^{3+}-doped heavy metal oxide glasses*. Chemical Physics Letters 408 (2005) 179-185.
10. Yang G.F., Q.Y. Zhang, T. Li, D.M. Shi, Z.H. Jiang, *"Laser-diode-excited intense luminescence and green-upconversion in erbium-doped bismuth-germanate-lead glasses"*. Spectrochimica Acta Part A: Mol. Biomol. Specrosc. (2007), doi: 10.1016/j.saa.2007.03.006.
11. Zhongmin Yang, Shiqing Xu, Lili Hu, Zhonghong Jiang, *"Density of Na_2O-(3-x)SiO_2-xGeO_2 glasses related to structure"*. Materials Research Bulletin 39 (2004) 217-222.
12. Ajroud M., M. Haouari, H. Ben Ouada, H. Măaref, A. Brenier, B. Champagnon, *"Energy transfer processes in (Er^{3+}-Yb^{3+})-codoped germanate glasses for mid-infrared and up-conversion applications"*. Materials Science and Engineering C 26 (2006) 523-529.
13. Fiorenzo Vetrone, John-Christopher Boyer, John A. Capobianco, Adolfo Speghini, Marco Bettinelli, *"980 nm excited upconversion in an Er-doped ZnO-TeO_2 glass"*. Applied Physics Letters Volume 80, Number 10 (2002) 1752-1754.
14. Kumar G.A., E. De La Rosa, H. Desirena, *"Radiative and non radiative spectroscopic properties of Er^{3+} ion in tellurite glass"*. Optics Communications 260 (2006) 601-606.
15. Meisong Liao, Shunguang Li, Hongtao Sun, Yongzheng Fang, Lili Hu And Junjie Zhang, *"Upconversion properties of Tm^{3+}/Yb^{3+} codoped fluorophosphate glasses with low phonon density of states"*. Materials Letters 60 (2006) 1783-1785.
16. Balda R., A. Oleaga, J. Fernández, J.M. Fdez-Navarro, *"Spectroscopy and frequency upconversion of Er^{3+} ions in lead niobium germanate glasses"*. Optical Materials 24 (2003) 83-90.
17. H Lin., K. Liu, E.Y.B. Pun, T.C. Ma, X. Peng, Q.D. An, J.Y. Yu, S.B. Jiang, *"Infrared and visible fluorescence in Er^{3+}-doped gallium tellurite glasses"*. Chemical Physics Letters 398 (2004) 146-150.
18. Hongtao Sun, Shiqing Xu, Shixun Dai, Junjie Zhang, Lili Hu, Zhonghong Jiang, *"Intense frequency upconversion fluorescence of Er^{3+}/Yb^{3+}-codoped novel potassium-barium-strontium-lead-bismuth glasses"*. Journal of Alloys and Compounds 391 (2005) 198-201.
19. Long Zhang, Hefang Hu, Changhong Qi, Fengying Lin, *"Spectroscopic properties and energy transfer in Yb^{3+}/Er^{3+}-doped phosphate glasses"*. Optical Materials 17 (2001) 371-377.
20. Zhongmin Yang, Shiqing Xu, Lili Hu, Zhonghong Jiang, *"Energy transfer and frequency upconversion in Yb^{3+}, Er^{3+} co-doped sodium-lead-germanate glasses"*. Journal of Alloys and Compounds 370 (2004) 94-98.
21. Yuan Gao, Qiu-Hua Nie, Tie-Feng Xu, Xiang Shen, *"Study of luminescence properties of novel Er^{3+} single-doped and Er^{3+}/Yb^{3+} co-doped tellurite glasses"*. Spectrochimica Acta Part A 61 (2005) 1259-1262.
22. Qiu-Hua Nie, Yuan Gao, Tie-Feng Xu, Xiang Shen, *"Investigation of thermal stability and spectroscopic properties in Er^{3+}/Yb^{3+}-codoped TeO_2-Li_2O-B_2O_3-GeO_2 glasses"*. Spectrochimica Acta Part A 61 (2005) 1939-1943.
23. Hongtao Sun, Shixun Dai, Shiqing Xu, Junjie Zhang, Lili Hu, Zhonghong Jiang, *"Efficient frequency upconversion emission of Er^{3+}/Yb^{3+}-codoped potassium-magnesium-lead-bismuth glasses pumped at 975 nm"*. Physica B 352 (2004) 366-371.
24. Zhang Q.Y., Z.M. Feng, Z.M. Yang, Z.H. Jiang, *"Energy transfer and infrared-to-visible upconversion luminescence of Er^{3+}/Yb^{3+}-codoped halide modified tellurite glasses"*. Journal of Quantitative Spectroscopy & Radiative Transfer 98 (2006) 167-179.
25. Padlyak B., O. Vlokh, K. Fabisiak, K. Sagoo, B. Kukliriski, *"Optical spectroscopy of the Er-doped glasses with $3CaO–Ga_2O_3–3GeO_2$ composition"*. Optical Materials 28 (2006) 157-161.
26. Hailian Liang, Kuisheng Yang, Xiyan Zhang, Ken-Ichi Machida, Jian Meng, *Up-conversion spectrum properties of the oxy-fluoride glass co-doped with Er^{3+} and Yb^{3+}"*. Journal of Alloys and Compounds 408-412 (2006) 835-837.
27. Uhlmann D. R., N. J. Kreidl, *"Glass Science and Technology"*, Vol. 4A, Acadmic Press Inc., (1990).
28. Stefan Nilsson-Gistvik, *"Optical Fiber Theory for Communication Networks"*, Ericsson Network Technologies AB, (2002).